

Discrete conservation properties for shallow water flows using mixed mimetic spectral elements

D. Lee^{a,*}, A. Palha^b, M. Gerritsma^c

^a*Computer, Computational and Statistical Sciences, Los Alamos National Laboratory, Los Alamos, NM 87545, USA*

^b*Eindhoven University of Technology, Department of Mechanical Engineering, P.O. Box 513, 5600 MB Eindhoven, The Netherlands*

^c*Delft University of Technology, Faculty of Aerospace Engineering, P.O. Box 5058, 2600 GB Delft, The Netherlands*

Abstract

A mixed mimetic spectral element method is applied to solve the rotating shallow water equations. The mixed method uses the recently developed spectral element edge functions, which exactly satisfy the fundamental theorem of calculus with respect to the standard Lagrange basis functions in one dimension, in order to construct tensor product solution spaces which satisfy the generalized Stokes theorem, as well as the annihilation of the gradient operator by the curl. This allows for the exact conservation of first order moments (mass, vorticity), as well as quadratic moments (energy, potential enstrophy), subject to the truncation error of the time stepping scheme. The continuity equation is solved in the strong form, such that mass conservation holds point wise, while the momentum equation is solved in the weak form such that vorticity is globally conserved. While mass, vorticity and energy conservation hold for any quadrature rule, potential enstrophy conservation is dependent on exact spatial integration. The method possesses several other properties desirable for geophysical fluid dynamics, including geostrophic balance in the weak form due to the compatible nature of the solution spaces, a 2/1 ratio of velocity to pressure degrees of freedom, such that there are two gravity wave solutions for every Rossby wave, and arbitrarily high order spatial accuracy.

Keywords: Mimetic, Spectral elements, High order, Shallow water, Energy and potential enstrophy conservation

1. Introduction

In recent years there has been much interest in the use of finite element methods for the development of geophysical fluid solvers. This is in large part due to the recognition of the importance of conservation over long time integrations as a means of mitigating against both numerical instabilities and biases in the solution [1], and the capacity of

*Corresponding author. Tel. +1 505 665 7286.

Email address: drlee@lanl.gov (D. Lee)

finite elements to satisfy the conservation of various moments via the use of compatible or mimetic finite element spaces [2]. Various finite element spaces have been explored for their suitability for modelling geophysical flows including Raviart-Thomas, Brezzi-Douglas-Marini and Brezzi-Douglas-Fortin-Marini elements [3, 4, 5]. When used in a sequence of element types such as the standard continuous and discontinuous Galerkin elements, these can be shown to exactly satisfy the Kelvin-Stokes and Gauss-divergence theorems when applying the curl and divergence operators respectively in the weak form, as well as the annihilation of the gradient operator by the curl. Satisfying these properties exactly in the discrete form is necessary in order to conserve both first and second order moments for the shallow water equations in rotational form, as first presented for a c-grid finite difference scheme [6].

The application of mimetic finite elements for shallow water flows has also been formalized in the language of exterior calculus in order to generalize the expression of their conservation properties [7]. Mimetic properties have also been demonstrated for the standard a-grid spectral element method on cubed sphere geometries via careful use of covariant and contravariant transformations in order to evaluate the curl and divergence operators respectively so as to exactly satisfy the Kelvin-Stokes and Gauss-divergence theorems [8].

The present study explores the use of mixed mimetic spectral elements for geophysical flows. These recently developed methods invoke the use of *edge* functions [9], which are defined such that they exactly satisfy the fundamental theorem of calculus with respect to the standard spectral element basis functions from which they are derived. In the language of exterior calculus these edge functions may then be regarded as defining the space of 1-forms (with the standard basis functions defining the space of 0-forms). By taking tensor product combinations of these basis functions and their associated edge functions higher dimensional differential k -forms may also be constructed for which the Kelvin-Stokes and Gauss-divergence theorems are satisfied [10].

Since these methods are designed specifically to satisfy the generalized Stokes theorem, differentiation may be defined abstractly as a topological mapping from lower to higher k -forms, independent of any notion of measure. Such mappings preserve the mimetic properties of the discretization point wise in the strong form. It is only when mapping from higher to lower forms via the co-differential operator, that the weak form of the problem and notions of measure need be invoked.

As for other compatible tensor product finite element methods, the mixed mimetic spectral elements provide an effective means of preserving many of the properties of a geophysical fluid over long time integrations. These include:

- *Conservation of mass, vorticity, total energy and potential enstrophy*

Conservation of mass ensures that the solution does not drift over time and develop large biases. Vorticity is an important moment to conserve since the large scale circulation of the atmosphere and oceans at mid latitudes is dominated by a quasi-balance between rotation and pressure gradients. Conservation of energy ensures that solutions remain bounded and numerical instabilities do not grow exponentially. The importance of potential enstrophy conservation is less immediately obvious meanwhile since for two dimensional turbulent fluids this cascades to small scales where some dissipation mechanism is necessary [11].

- *Stationary geostrophic modes*

The large scale circulations of the atmosphere and ocean are dominated by the slow evolution of modes balanced between Coriolis forces and pressure gradients. If this balance cannot be exactly replicated in a numerical model then the process of adjustment will result in the radiation of fast gravity waves that can contaminate the solution [12].

- *2/1 ratio of velocity to pressure degrees of freedom*

This ensures that in the discrete eigenvalue problem for the linearized shallow water system there will be two gravity modes for every Rossby mode. If there are less than 2 velocity degrees of freedom (dof) for every pressure dof then there will be spurious fast gravity waves which can contaminate the solution. If there are more than 2 velocity dofs for every pressure dof then there will be spurious Rossby waves [13]. While these are slow moving and so less likely to contaminate the solution than spurious gravity waves, they are none the less unphysical and so best avoided.

- *High order spatial accuracy*

The spectral element method defines the nodes of the basis functions to cluster towards element boundaries such that spurious oscillations due to spectral ringing are avoided, allowing convergence at arbitrarily high order accuracy.

The rest of this paper proceeds as follows: In the following section the mixed mimetic spectral element, as introduced by previous authors [9, 10, 14, 15] will be briefly discussed. For a more detailed discussion the reader is referred to the references therein. In Section 3 the solution of the rotating shallow water equations using the mixed mimetic spectral element method will be detailed, including the conservation properties of the discrete system. In Section 4 some results are presented, demonstrating the error convergence, conservation and balance properties of the method. Section 5 details some conclusions regarding the suitability of the method for geophysical flows, its advantages and limitations.

2. Mixed mimetic spectral elements

The mixed mimetic spectral elements are constructed via the use of *nodal* and *edge* functions [9]. As the name suggests, these edge functions, $e_i(\xi)$ integrate to one on one edge and to zero on all other edges,

$$\int_{\xi_{j-1}}^{\xi_j} e_i(\xi) = \begin{cases} 1 & \text{if } i = j \\ 0 & \text{if } i \neq j \end{cases} \quad (1)$$

while the nodal basis functions, $l_i(\xi)$ evaluate to one in one node and zero at all other nodes

$$l_i(\xi_j) = \begin{cases} 1 & \text{if } i = j \\ 0 & \text{if } i \neq j \end{cases} . \quad (2)$$

The edge functions are defined such that in 1D the exterior derivative d acting on a 0-form variable of polynomial degree N ,

$$f^{(0)}(\xi) = \sum_{i=0}^N a_i^{(0)} l_i(\xi) \quad (3)$$

exactly maps to the space of 1-forms in such a way that the fundamental theorem of calculus is preserved between two nodes ξ_i and ξ_{i+1} [16] as,

$$df^{(0)} = d \sum_{i=0}^N a_i^{(0)} l_i(\xi) = \sum_{i=1}^N (a_i^{(0)} - a_{i-1}^{(0)}) e_i(\xi) d\xi \quad (4)$$

where the application of the exterior derivative to the coordinate ξ raises this to a 1-form. In this fashion the fundamental theorem of calculus is satisfied exactly in a purely topological fashion that allows for the exterior derivative to be defined abstractly without any reference to the geometry of the problem. Henceforth we assume the use of Lagrange polynomials for the 0-form basis, defined for polynomial degree N as

$$l_i(\xi) = \prod_{j=0, j \neq i}^N \frac{(\xi - \xi_j)}{(\xi_i - \xi_j)} \quad (5)$$

for the Gauss-Lobatto points ξ_j . The 1-form edge functions are then given so as to satisfy (4) as [9]

$$e_i(\xi) = - \sum_{j=0}^{i-1} \frac{dl_j(\xi)}{d\xi}. \quad (6)$$

In higher dimensions we can use the same procedure to exactly satisfy the Kelvin-Stokes and Gauss-divergence theorems by taking tensor product combinations of $l_i(\xi)$ and $e_i(\xi)$ such that in 2D the different k -forms are defined across a given element as

$$\alpha_{i,j}^{(0)}(\xi, \eta) = l_i(\xi) \otimes l_j(\eta) \in V^{(0)} \quad (7)$$

$$\beta_{i,j}^{(1)}(\xi, \eta) = \{\beta_{i,j}^{(1),\xi}(\xi, \eta), \beta_{i,j}^{(1),\eta}(\xi, \eta)\} = \{l_i(\xi) \otimes e_j(\eta) d\eta, e_i(\xi) d\xi \otimes l_j(\eta)\} \in V^{(1)} \quad (8)$$

$$\gamma_{i,j}^{(2)}(\xi, \eta) = e_i(\xi) d\xi \otimes e_j(\eta) d\eta \in V^{(2)}. \quad (9)$$

We assume that 0-forms, 1-forms and 2-forms may be represented by the expansions

$$\psi^{(0)}(\xi, \eta) = \sum_{i,j} a_{i,j}^{(0)} \alpha_{i,j}^{(0)}(\xi, \eta) \quad (10)$$

$$u^{(1)}(\xi, \eta) = \sum_{i,j} b_{i,j}^{(1),\xi} \beta_{i,j}^{(1),\xi}(\xi, \eta) + \sum_{i,j} b_{i,j}^{(1),\eta} \beta_{i,j}^{(1),\eta}(\xi, \eta) \quad (11)$$

$$\rho^{(2)}(\xi, \eta) = \sum_{i,j} c_{i,j}^{(2)} \gamma_{i,j}^{(2)}(\xi, \eta) \quad (12)$$

respectively. Then using (4) the exterior derivative mapping from the 0-form to the 1-form manifold and the 1-form to the 2-form manifold are given as

$$d\psi_{i,j}^{(0)}(\xi, \eta) = \{(a_{i,j}^{(0)} - a_{i,j+1}^{(0)})l_i(\xi)e_j(\eta)d\eta, (a_{i+1,j}^{(0)} - a_{i,j}^{(0)})e_i(\xi)l_j(\eta)d\xi\} \quad (13)$$

$$= \{b_{i,j}^{(1),\xi}l_i(\xi)e_j(\eta)d\eta, b_{i,j}^{(1),\eta}e_i(\xi)l_j(\eta)d\xi\} \quad (14)$$

$$= \{u_{i,j}^{(1),\xi}(\xi, \eta), u_{i,j}^{(1),\eta}(\xi, \eta)\} \quad (15)$$

$$du_{i,j}^{(1)}(\xi, \eta) = (b_{i+1,j}^{(1),\xi} - b_{i,j}^{(1),\xi} + b_{i,j+1}^{(1),\eta} - b_{i,j}^{(1),\eta})e_i(\xi)e_j(\eta)d\xi d\eta \quad (16)$$

$$= c_{i,j}^{(2)}e_i(\xi)e_j(\eta)d\xi d\eta \quad (17)$$

$$= \rho_{i,j}^{(2)}(\xi, \eta) \quad (18)$$

These operations are the equivalent of $\nabla^\perp \psi = \vec{u}$ and $\nabla \cdot \vec{u} = \rho$ as given by standard vector calculus.

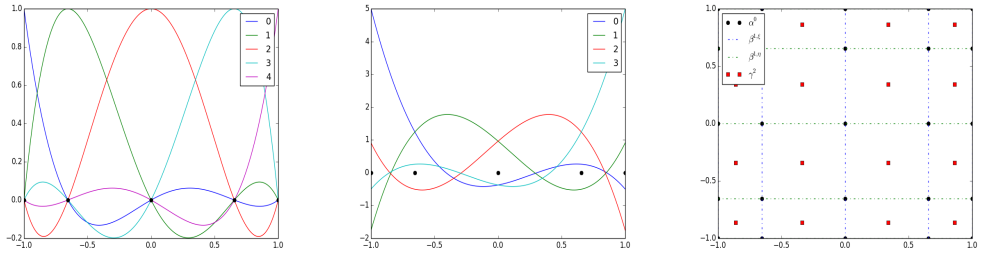


Fig. 1: Lagrange polynomial (0-form) basis functions (left), associated edge (1-form) basis functions, (center) and 2D tensor product bases for the 0-form (node), 1-form (edge) and 2-form (face) spaces (right). Gauss-Lobatto quadrature points are shown in black.

As can be seen from the above relations, the application of the exterior derivative leads to a purely topological relation between k -forms. We represent this by the matrix $E^{k,k-1}$ [10], which defines the orientation of the discrete edges ($k = 1$) or cells ($k = 2$) of the k form manifold (called k -chains) with respect to the neighbouring vertices ($k-1 = 0$) or edges ($k-1 = 1$) of the $k-1$ form manifold. The data which resides on these k -chains is referred to as co-chains. As for the regular exterior derivative, the property $d \circ d := 0$ holds for the discrete operator, such that $E^{k+1,k}E^{k,k-1} = 0$. This is the discrete exterior calculus form of the vector calculus identities $\nabla \times \nabla := 0$ and $\nabla \cdot \nabla^\perp := 0$. Since the exterior derivative is represented in a purely topological manner using tensor product spaces, the discrete exterior derivative from higher to lower k -forms, d^* , is given simply by the transpose of $E^{k,k-1}$, such that $E_{k-1,k} = (E^{k,k-1})^T$ (where \star represents the Hodge-star operator which maps from k -forms to $(n-k)$ -forms in an n dimensional space).

The exterior derivative mapping from lower to higher forms satisfies the generalized Stokes theorem exactly in the strong form and holds point wise. This is given as [17]

$$\int_{\Omega^{(k)}} d\alpha^{(k-1)} = \int_{\partial\Omega^{(k)}} \alpha^{(k-1)} \quad (19)$$

where $\partial\Omega^{(k)}$ denotes the $(k-1)$ -dimensional boundary of a k -dimensional domain. In the absence of a dual mesh and an explicitly defined discrete Hodge- \star operator [18], the

discrete co-differential operator $d^* := (-1)^{n(k+1)+1} \star d\star$, [10, 14, 15, 17], is defined as

$$(\alpha_h^{(k-1)}, d^* \beta_h^{(k)})_{\Omega_a} := (d\alpha_h^{(k-1)}, \beta_h^{(k)})_{\Omega_a} - \int_{\partial\Omega_a} \alpha_h^{(k-1)} \wedge \star \beta_h^{(k)} \quad (20)$$

$$= E_{k-1,k}(\beta_h^{(k)}, \beta_h^{(k)})_{\Omega_a} - \int_{\partial\Omega_a} \alpha_h^{(k-1)} \wedge \star \beta_h^{(k)}. \quad (21)$$

where \wedge represents the wedge product which takes a k - and an l - form as inputs and returns a $(k+l)$ form. The adjoint relation as given in (20) is equivalent to the standard vector calculus procedure of integrating by parts, as used in regular finite element methods. The one difference here, that results from this particular choice of function spaces, is that the exterior derivative of a $(k-1)$ -form test function $\alpha_h^{(k-1)}$ can be expressed as a linear combination of k -form test functions $\beta_h^{(k)}$. In this way, the generalized Stokes theorem is satisfied exactly at the discrete level and the degrees of freedom of the k - and $(k-1)$ -forms are related in a purely topological way by the incidence matrix $E_{k-1,k}$.

In this section we have very briefly outlined the practical details required to implement the mixed mimetic spectral element method in both the weak and strong form. This method draws from a rich background of differential forms, exterior calculus and algebraic topology. For a more detailed reading of this method the reader is referred to the work of previous authors [9, 10, 14, 15] and the references therein.

3. Discretization and solution of the shallow water equations

The shallow water equations present an excellent testing ground for primitive equation atmospheric and oceanic models since they exhibit many of the same features, including slowly evolving Rossby waves and fast gravity waves, nonlinear cascades of kinetic energy to large scales and potential enstrophy to small scales, and the conservation of various moments (mass, total energy, vorticity, and an infinite number of rotational moments, of which potential enstrophy is the first). These are given in rotational form using vector calculus as [6]

$$\frac{\partial \vec{u}}{\partial t} + q \times \vec{F} + \nabla(K + gh) = 0 \quad (22)$$

$$\frac{\partial h}{\partial t} + \nabla \cdot \vec{F} = 0 \quad (23)$$

where \vec{u} and h are the prognostic variables of velocity and fluid depth respectively. The diagnostic variables are the potential vorticity $q = (\omega + f)/h$ (where $\omega = \nabla \times \vec{u}$ is the vorticity and f the Coriolis term), the mass flux $\vec{F} = h\vec{u}$, and the kinetic energy per unit mass $K = \vec{u} \cdot \vec{u}$.

We assume an outer oriented (normal velocity) discretization of these equations with $f^{(n-2)}, q^{(n-2)}$ and $\omega^{(n-2)} = -d^* u^{(n-1)} \in V^{(n-2)}$ with C_0 continuity between elements, $u^{(n-1)}, F^{(n-1)} \in V^{(n-1)}$ as outer oriented co-chains with C_0 continuous normal components and $h^{(n)}, K^{(n)} \in V^{(n)}$ and discontinuous at element boundaries. Here n represents the dimension of the domain (hereafter $n = 2$). This is in keeping with a traditional c-grid finite difference discretization [6], where rotational moments are located at vertices, normal velocities on edges and pressure and mass variables at cell centers. A d-grid

analogue also exists, for which the tangential and not the normal velocities reside on the edges. The differential forms formulation of the shallow water equations is then given as

$$\frac{\partial u^{(n-1)}}{\partial t} + \star(q^{(n-2)} \wedge F^{(n-1)}) - d^*(K^{(n)} + gh^{(n)}) = 0 \quad (24)$$

$$\frac{\partial h^{(n)}}{\partial t} + dF^{(n-1)} = 0 \quad (25)$$

where

$$\star(h^{(n)} \wedge q^{(n-2)}) = -d^*u^{(n-1)} + f^{(n-2)}, \quad (26)$$

$$F^{(n-1)} = \star h^{(n)} \wedge u^{(n-1)}, \quad (27)$$

and [7]

$$K^{(n)} = \frac{1}{2}u^{(n-1)} \wedge \star u^{(n-1)}. \quad (28)$$

Note that the diagnostic equations (26-28) include Hodge-star operators applied to $\star h^{(2)}$ and $\star u^{(1)}$. This ensures that the resulting nonlinear terms correspond to the correct k -forms for the respective equations. We evaluate these terms by analytically computing the Hodge-star operators on the original series expansions (7-9).

The nonlinear potential vorticity diagnostic equation (26) may be solved via a Galerkin projection onto the 0-form test functions $\alpha_h^{(0)}$ as

$$(\alpha_h^{(0)}, \star(h_h^{(2)} \wedge q_h^{(0)}))_{\Omega_a} = -(\alpha_h^{(0)}, d^*u_h^{(1)})_{\Omega_a} + (\alpha_h^{(0)}, f_h^{(0)})_{\Omega_a}. \quad (29)$$

Note the change of sign in the first term on the right hand side compared to the standard vector calculus definition. This is due to the definition of the adjoint operator $d^* = -\star d \star$ for $n = 2$ [10, 14]. We then apply the adjoint relation (20) as

$$(\alpha_h^{(0)}, \star(h_h^{(2)} \wedge q_h^{(0)}))_{\Omega_a} = -(d\alpha_h^{(0)}, u_h^{(1)})_{\Omega_a} + (\alpha_h^{(0)}, f_h^{(0)})_{\Omega_a}, \quad (30)$$

where we have assumed periodic boundary conditions and so have omitted the boundary integral associated with the adjoint relation. Recalling that the exterior derivative is a purely topological operator and so may be taken outside the integral, the weak form may be given as

$$(\alpha_h^{(0)}, \star(h_h^{(2)} \wedge \alpha_h^{(0)}))_{\Omega_a} \tilde{q}_h^{(0)} = -E_{0,1}(\beta_h^{(1)}, \beta_h^{(1)})_{\Omega_a} \tilde{u}_h^{(1)} + (\alpha_h^{(0)}, f_h^{(0)})_{\Omega_a} \quad (31)$$

where $\tilde{q}_h^{(0)}$ and $\tilde{u}_h^{(1)}$ correspond to the degrees of freedom in the series expansions of $q_h^{(0)}$ and $u_h^{(1)}$ respectively.

The diagnostic equations for $F^{(1)}$ and $K^{(2)}$ (27,28) represent nonlinear Galerkin projections onto the space of 1-forms and 2-forms respectively. These may be given as

$$(\beta_h^{(1)}, F_h^{(1)})_{\Omega_a} = (\beta_h^{(1)}, \star h_h^{(2)} \wedge u_h^{(1)})_{\Omega_a} \quad (32)$$

$$(\gamma_h^{(2)}, K_h^{(2)})_{\Omega_a} = \frac{1}{2}(\gamma_h^{(2)}, u_h^{(1)} \wedge \star u_h^{(1)})_{\Omega_a}. \quad (33)$$

Once we have determined the discrete diagnostic quantities $q_h^{(0)}$, $F_h^{(1)}$ and $K_h^{(2)}$ we are free to solve the original shallow water system. In order to solve for the momentum equation (24), we first multiply by the 1-form test functions and integrate over each element as

$$\frac{d}{dt}(\beta_h^{(1)}, u_h^{(1)})_{\Omega_a} = -(\beta_h^{(1)}, \star(q_h^{(0)} \wedge F_h^{(1)}))_{\Omega_a} + (\beta_h^{(1)}, d^*(K_h^{(2)} + gh_h^{(2)}))_{\Omega_a} \quad (34)$$

$$= -(\beta_h^{(1)}, \star(q_h^{(0)} \wedge F_h^{(1)}))_{\Omega_a} + (d\beta_h^{(1)}, K_h^{(2)} + gh_h^{(2)})_{\Omega_a}. \quad (35)$$

We then have the final expression for the momentum equation as

$$\frac{d}{dt}(\beta_h^{(1)}, \beta_h^{(1)})_{\Omega_a} \tilde{u}_h^{(1)} = -(\beta_h^{(1)}, \star(q_h^{(0)} \wedge F_h^{(1)}))_{\Omega_a} + E_{1,2}(\gamma_h^{(2)}, \gamma_h^{(2)})_{\Omega_a} (\tilde{K}_h^{(2)} + g\tilde{h}_h^{(2)}). \quad (36)$$

Unlike the momentum equation (24), the mass equation (25) involves an exterior derivative mapping from the lower 1-form $F_h^{(1)}$ to the 2-form fluid depth $h_h^{(2)}$. This can be done in the strong form without the need to apply a Galerkin projection, and is given simply as

$$\frac{dh_h^{(2)}}{dt} = -E^{2,1}F_h^{(1)}. \quad (37)$$

Equation (37) satisfies the divergence theorem exactly for every 1-form and 2-form k chain such that mass is conserved point wise.

We solve the system (36, 37) using Runge-Kutta time integrators of varying order. Using such an explicit method total energy and potential enstrophy are conserved only in the limit as $\Delta t \rightarrow 0$, however the errors in total energy and potential enstrophy conservation converge with the order of the time stepping scheme. The conservation of energy holds for inexact spatial integration, while the conservation of potential enstrophy is subject to exact integration of the nonlinear terms. These properties will be discussed in the following sections. We use Gauss-Lobatto quadrature, which is exact for order $2N - 1$ polynomials.

3.1. Conservation of mass

Mass conservation is exactly satisfied by (37) since the divergence theorem as encoded by the discrete exterior derivative $E^{1,2}$, and given in (19) with $k = 2$, is exact.

3.2. Conservation of vorticity

The argument for vorticity conservation closely follows that for standard compatible finite elements [4]. Since (36) holds for all 1-forms $\beta_h^{(1)}$, then it certainly holds for $\beta_h^{(1)} = d\alpha_h^{(0)}$, which yields

$$\frac{d}{dt}(d\alpha_h^{(0)}, u_h^{(1)})_{\Omega_a} = -(d\alpha_h^{(0)}, \star(q_h^{(0)} \wedge F_h^{(1)}))_{\Omega_a} + (dd\alpha_h^{(0)}, K_h^{(2)} + gh_h^{(2)})_{\Omega_a}. \quad (38)$$

The second term on the right hand side is exactly zero since the identity $dd \equiv 0$ holds in the discrete form as $E^{2,1}E^{1,0} = 0$, such there is no spurious projection from the 2-form

energy space onto the 0-form vorticity space. We then may apply the adjoint relation to the left hand side (assuming periodic boundary conditions) such that

$$\frac{d}{dt}(\alpha_h^{(0)}, d^*u_h^{(1)})_{\Omega_a} = -(d\alpha_h^{(0)}, \star(q_h^{(0)} \wedge F_h^{(1)}))_{\Omega_a}. \quad (39)$$

Since $(\alpha_h^{(0)}, \omega_h^{(0)})_{\Omega_a} = -(\alpha_h^{(0)}, d^*u_h^{(1)})_{\Omega_a} = -E_{0,1}(\beta_h^{(1)}, \beta_h^{(1)})_{\Omega_a} \tilde{u}_h^{(1)}$ is the vorticity as defined in the weak form (with periodic boundary conditions), (39) gives an expression for vorticity conservation which holds globally. We can make this explicit by setting $\alpha_h^{(0)} = 1$ such that

$$\frac{d}{dt}(1, \omega_h^{(0)})_{\Omega_a} = 0. \quad (40)$$

Note that the conservation of vorticity is satisfied irrespective of whether $q_h^{(0)}$ is the same on the left hand side of (39) as the right. As such vorticity conservation is preserved in the event that the anticipated potential vorticity method [19] is used to truncate the potential enstrophy cascade, since this involves removing some downstream *anticipated* potential vorticity from the right hand side in order to introduce some dispersion into the vorticity advection equation. We construct this anticipated potential vorticity $\hat{q}_h^{(0)}$ in the weak form as

$$(\alpha_h^{(0)}, \hat{q}_h^{(0)})_{\Omega_a} = \Delta\tau(\alpha_h^{(0)}, u_h^{(1)} \wedge dq_h^{(0)})_{\Omega_a} \quad (41)$$

where $\Delta\tau$ is some time scale associated with the evaluation of the downstream potential vorticity.

3.3. Conservation of energy

We assume a weak formulation of total energy E as a Galerkin projection onto $h_h^{(2)}$ as

$$\frac{dE}{dt} = \frac{d}{dt} \left(h_h^{(2)}, K_h^{(2)} + \frac{1}{2}gh_h^{(2)} \right)_{\Omega_a} = 0. \quad (42)$$

Following the derivation for energy conservation for both regular finite and spectral elements [4, 8], we begin by expanding (42) via the chain rule as

$$\left(h_h^{(2)}, \frac{dK_h^{(2)}}{dt} \right)_{\Omega_a} + \left(\frac{dh_h^{(2)}}{dt}, K_h^{(2)} \right)_{\Omega_a} + \left(\frac{dh_h^{(2)}}{dt}, gh_h^{(2)} \right)_{\Omega_a} = 0. \quad (43)$$

Setting $\gamma_h^{(2)} = h_h^{(2)}$ in (33), which is permitted since $\gamma_h^{(2)}, h_h^{(2)} \in V^{(2)}$, the first term is then given as

$$\left(h_h^{(2)}, \frac{1}{2} \frac{du_h^{(1)} \wedge \star u_h^{(1)}}{dt} \right)_{\Omega_a} + \left(\frac{dh_h^{(2)}}{dt}, K_h^{(2)} \right)_{\Omega_a} + \left(\frac{dh_h^{(2)}}{dt}, gh_h^{(2)} \right)_{\Omega_a} = 0. \quad (44)$$

Since both the domain of the problem and the mesh do not change in time, the time derivative commutes with the Hodge- \star operator. Therefore we can rewrite the first term on the left hand side of (44) as

$$\left(h_h^{(2)}, \frac{1}{2} \frac{du_h^{(1)} \wedge \star u_h^{(1)}}{dt}\right)_{\Omega_a} = \frac{1}{2} \left(h_h^{(2)}, \frac{du_h^{(1)}}{dt} \wedge \star u_h^{(1)}\right)_{\Omega_a} + \frac{1}{2} \left(h_h^{(2)}, u_h^{(1)} \wedge \star \frac{du_h^{(1)}}{dt}\right)_{\Omega_a} \quad (45)$$

$$= \left(h_h^{(2)}, u_h^{(1)} \wedge \star \frac{du_h^{(1)}}{dt}\right)_{\Omega_a}. \quad (46)$$

The expression in (46) can be re-written as

$$\left(h_h^{(2)}, u_h^{(1)} \wedge \star \frac{du_h^{(1)}}{dt}\right)_{\Omega_a} := \int_{\Omega_a} \star h_h^2 \wedge u^1 \wedge \star \frac{du^1}{dt} d\Omega_a = \left(\star h_h^{(2)} \wedge u_h^{(1)}, \frac{du_h^{(1)}}{dt}\right)_{\Omega_a} \quad (47)$$

Substituting (47) into (44) yields

$$\left(\star h_h^{(2)} \wedge u_h^{(1)}, \frac{du_h^{(1)}}{dt}\right)_{\Omega_a} + \left(\frac{dh_h^{(2)}}{dt}, K_h^{(2)}\right)_{\Omega_a} + \left(\frac{dh_h^{(2)}}{dt}, gh_h^{(2)}\right)_{\Omega_a} = 0. \quad (48)$$

Setting $\beta_h^{(1)} = du_h^{(1)}/dt$ in (32) and substituting this into the first term gives

$$\left(F_h^{(1)}, \frac{du_h^{(1)}}{dt}\right)_{\Omega_a} + \left(\frac{dh_h^{(2)}}{dt}, K_h^{(2)}\right)_{\Omega_a} + \left(\frac{dh_h^{(2)}}{dt}, gh_h^{(2)}\right)_{\Omega_a} = 0. \quad (49)$$

In order to show that these terms balance exactly, we set $\beta_h^{(1)} = F_h^{(1)}$ in (35) such that

$$\left(F_h^{(1)}, \frac{du_h^{(1)}}{dt}\right)_{\Omega_a} = -(F_h^{(1)}, \star(q_h^{(0)} \wedge F_h^{(1)}))_{\Omega_a} + (dF_h^{(1)}, K_h^{(2)} + gh_h^{(2)})_{\Omega_a}. \quad (50)$$

The first term on the right hand exactly cancels since $F_h^{(1)}$ is exactly perpendicular to $\star(q_h^{(0)} \wedge F_h^{(1)})$. Substituting $\gamma_h^{(2)} = K_h^{(2)}$ and $\gamma_h^{(2)} = gh_h^{(2)}$ and applying a Galerkin projection of the discrete continuity equation (37) onto these spaces respectively gives

$$\left(\frac{dh_h^{(2)}}{dt}, K_h^{(2)}\right)_{\Omega_a} = -(dF_h^{(1)}, K_h^{(2)})_{\Omega_a} \quad (51)$$

$$\left(\frac{dh_h^{(2)}}{dt}, gh_h^{(2)}\right)_{\Omega_a} = -(dF_h^{(1)}, gh_h^{(2)})_{\Omega_a}. \quad (52)$$

Substituting (50-52) into (49) shows that total energy is conserved in the weak form, and that this is true for both exact and inexact integration, provided that the same quadrature and interpolation rules are used for $F_h^{(1)}$ and $K_h^{(2)}$ in each equation. Note however that we require that the quadratic term $u_h^{(1)} \wedge \star u_h^{(1)}$ commutes with the time derivative in the weak form going from (44) to (48). The argument therefore is true only to truncation error in the time integration scheme.

3.4. Conservation of potential enstrophy

Potential enstrophy is defined in the weak form as [4] $Q = (q_h^0, \star(h_h^2 \wedge q_h^0))_{\Omega_a}$. Differentiating in time and expanding via the chain rule gives

$$\frac{d}{dt}(q_h^{(0)}, \star(h_h^{(2)} \wedge q_h^{(0)}))_{\Omega_a} = 2\left(q_h^{(0)}, \star\frac{d}{dt}(h_h^{(2)} \wedge q_h^{(0)})\right)_{\Omega_a} - \left(q_h^{(0)} \wedge q_h^{(0)}, \star\frac{dh_h^{(2)}}{dt}\right)_{\Omega_a}. \quad (53)$$

If we take the time derivative of (29) and assume that the Coriolis term is constant in time we obtain

$$\left(\alpha_h^{(0)}, \star\frac{d}{dt}(h_h^{(2)} \wedge q_h^{(0)})\right)_{\Omega_a} = \left(\alpha_h^{(0)}, \frac{d}{dt}d^*u_h^{(1)}\right)_{\Omega_a}. \quad (54)$$

By applying integration by parts to the right hand side and using (35) with $\beta_h^{(1)} = d\alpha_h^{(0)}$ we can rewrite (54) as

$$\left(\alpha_h^{(0)}, \star\frac{d}{dt}(h_h^{(2)} \wedge q_h^{(0)})\right)_{\Omega_a} = -\left(\alpha_h^{(0)}, \frac{d}{dt}d^*u_h^{(1)}\right)_{\Omega_a} \quad (55)$$

$$= (d\alpha_h^{(0)}, \star(q_h^{(0)} \wedge F_h^{(1)}))_{\Omega_a}. \quad (56)$$

If we now set $\alpha_h^{(0)} = q_h^{(0)}$ we obtain

$$\left(q_h^{(0)}, \star\frac{d}{dt}(h_h^{(2)} \wedge q_h^{(0)})\right)_{\Omega_a} = (dq_h^{(0)}, \star(q_h^{(0)} \wedge F_h^{(1)}))_{\Omega_a}. \quad (57)$$

Rearranging the term on the right hand side we can write (57) as

$$\left(q_h^{(0)}, \star\frac{d}{dt}(h_h^{(2)} \wedge q_h^{(0)})\right)_{\Omega_a} = \frac{1}{2}(\star F_h^{(1)}, d(q_h^{(0)} \wedge q_h^{(0)}))_{\Omega_a}. \quad (58)$$

Substituting (58) into (53) yields

$$\frac{d}{dt}(q_h^{(0)}, \star(h_h^{(2)} \wedge q_h^{(0)}))_{\Omega_a} = (\star F_h^{(1)}, d(q_h^{(0)} \wedge q_h^{(0)}))_{\Omega_a} - \left(q_h^{(0)} \wedge q_h^{(0)}, \star\frac{dh_h^{(2)}}{dt}\right)_{\Omega_a}. \quad (59)$$

If we now use (25) on the second term on the right hand side of (59) we obtain

$$\frac{d}{dt}(q_h^{(0)}, \star(h_h^{(2)} \wedge q_h^{(0)}))_{\Omega_a} = (\star F_h^{(1)}, d(q_h^{(0)} \wedge q_h^{(0)}))_{\Omega_a} + (q_h^{(0)} \wedge q_h^{(0)}, \star d F_h^{(1)})_{\Omega_a}. \quad (60)$$

Using the definition of the inner product and rearranging gives

$$\frac{d}{dt}(q_h^{(0)}, \star(h_h^{(2)} \wedge q_h^{(0)}))_{\Omega_a} = \int_{\Omega_a} d(q_h^{(0)} \wedge q_h^{(0)} \wedge F_h^{(1)}) = \int_{d\Omega_a} q_h^{(0)} \wedge q_h^{(0)} \wedge F_h^{(1)} = 0. \quad (61)$$

Note that for the above argument to hold the quadratic term $q_h^0 \wedge q_h^0$ must commute with both the temporal and spatial derivatives in the weak form. Therefore potential enstrophy conservation, like energy conservation, holds only to the order of the time integration scheme. However unlike energy conservation, potential enstrophy conservation is also contingent on exact spatial integration.

3.5. Geostrophic balance

The existence of stationary geostrophic modes derives from the linearized system [3]

$$\frac{\partial u^{(1)}}{\partial t} + \star(f^{(0)} \wedge u^{(1)}) - gd^*h^{(2)} = 0 \quad (62)$$

$$\frac{\partial h^{(2)}}{\partial t} + Hdu^{(1)} = 0 \quad (63)$$

where H is the mean depth of the fluid layer. If we assume a stationary solution then we have the balanced system

$$\star(f^{(0)} \wedge u^{(1)}) - gd^*h^{(2)} = 0 \quad du^{(1)} = 0. \quad (64)$$

This property is exactly satisfied by the compatible spectral element discretization as the co-differential of the 2-form $h^{(2)}$ space maps into the 1-form velocity space $u^{(1)}$ in the weak form as

$$(\beta_h^{(1)}, \star(f_h^{(0)} \wedge u_h^{(1)}))_{\Omega_a} = E_{1,2}(\gamma_h^{(2)}, \gamma_h^{(2)})_{\Omega_a} \tilde{h}_h^{(2)}. \quad (65)$$

Beyond the preservation of exact balances and conservation in the discrete compatible spectral element discretization, the system also has an exact ratio of 2 velocity degrees of freedom for every pressure (or fluid depth for the hydrostatically balanced case) degree of freedom due to the construction of bases as quadrilateral tensor products.

4. Results

4.1. Convergence

Before testing the full shallow water solver we validate the L_2 norm error convergence of the operators. For this we compare the three diagnostic equations (31-33) to the analytic solutions for a specified velocity and depth field, as derived from a stream function solution of

$$\psi = e^{-2.5((x-\pi)^2 + (y-2\pi/3)^2)} + e^{-2.5((x-\pi)^2 + (y-4\pi/3)^2)} \quad 0 \leq x, y < 2\pi, \quad (66)$$

where the velocity is given as $\vec{u} = \nabla^\perp \psi$, and the depth is derived from geostrophic balance as $f \times \vec{u} + g\nabla h = 0$, with $f = g = H = 8.0$ (and H being the constant of integration in the geostrophic balance relation). By validating both the algebraic convergence of the errors for constant polynomial degree with decreasing mesh size and the spectral convergence with increasing polynomial degree and constant mesh size of the solution for each of the diagnostic equations at varying grid resolutions we are able to validate the basis functions for each of the 0, 1 and 2-form function spaces.

As shown in Fig. (2), $q_h^{(0)}$, $F_h^{(1)}$ and $K_h^{(2)}$ all converge at the desired order of accuracy for both 4th and 5th order accurate basis representations. Moreover spectral accuracy is also observed for the convergence of errors with constant mesh size and increasing polynomial order. This shows that the 0-form, 1-form and 2-form tensor product elements all demonstrate spectral error convergence.

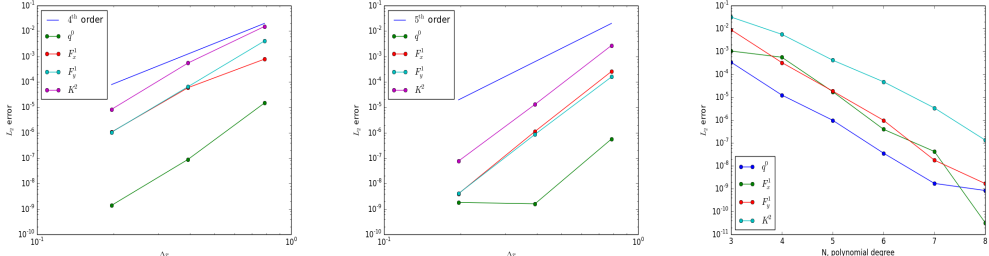


Fig. 2: Algebraic convergence for the 3rd order (left) and 4th order (center) basis functions for $q^{(0)}$, $F^{(1)}$ and $K^{(2)}$, and spectral convergence with polynomial degree (right). Blue slopes show the theoretical convergence rates for 4th and 5th order respectively.

4.2. Conservation

The model is tested for a pair of vortices starting in approximate geostrophic balance, as given from the stream function solution in (66). The solution behaves as expected, with fast gravity waves radiating out from the initial disturbance, which is preserved for long times due to the approximate geostrophic balance of the initial condition, as shown in Fig. (3).

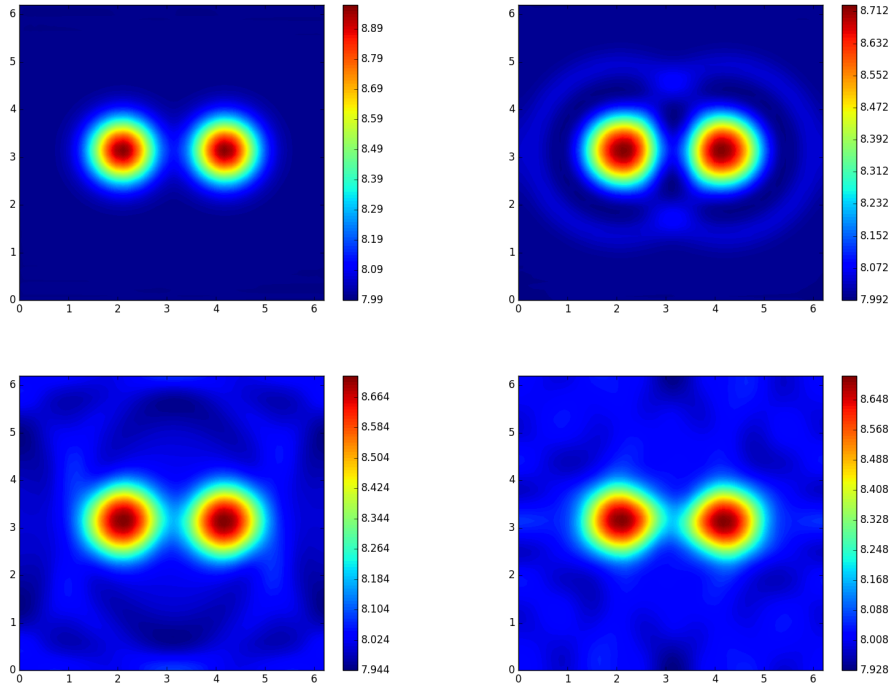


Fig. 3: Fluid depth h at times $t = 0.0, 0.5, 1.0$ and 2.0 dimensionless units. Approximate geostrophic balance is preserved while fast gravity waves radiate outwards from the disturbances.

As discussed, mass and vorticity conservation hold independent of time step, as shown in Fig. (4). This is due to the point wise satisfaction of the divergence theorem in the case of mass, and the elimination of the gradient operator by the curl in the weak form in the case of vorticity. Total energy and potential enstrophy are conserved to truncation error in time, as shown in Fig. (5), with the second order Runge-Kutta time stepping scheme applied with varying time step size. While energy conservation holds for inexact spatial integration, due to the exact cancellation of errors independent of quadrature order, potential enstrophy conservation fails for inexact integration, as shown in Fig. (6).

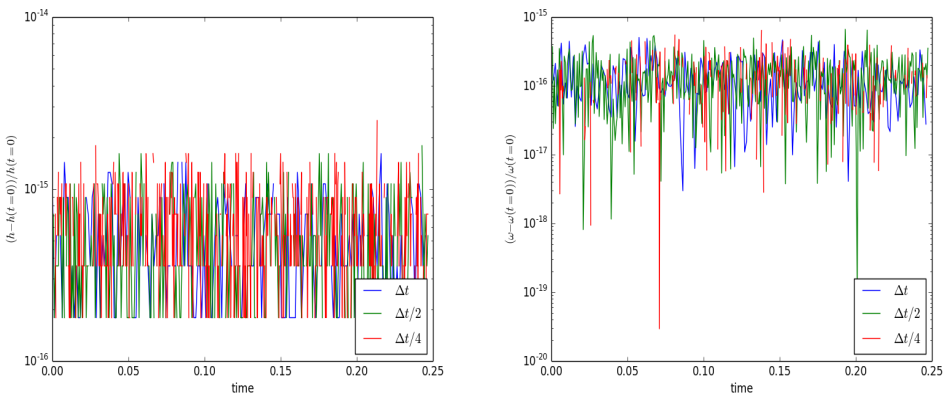


Fig. 4: Exact conservation for the volume, h (left) and vorticity, ω (right) with time.

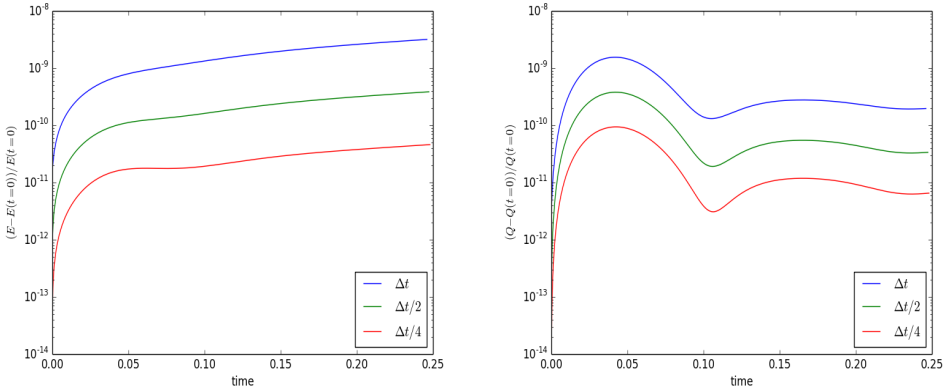


Fig. 5: Convergence of conservation errors for the energy, E (left) and potential enstrophy, Q (right) with time step Δt (exact spatial integration).

4.3. Shear flow over a mountain

As a final test we solve for a shear flow initial condition over a stationary orographic feature. The orography is implemented as a 2-form $b_h^{(2)}$, such that the momentum equa-

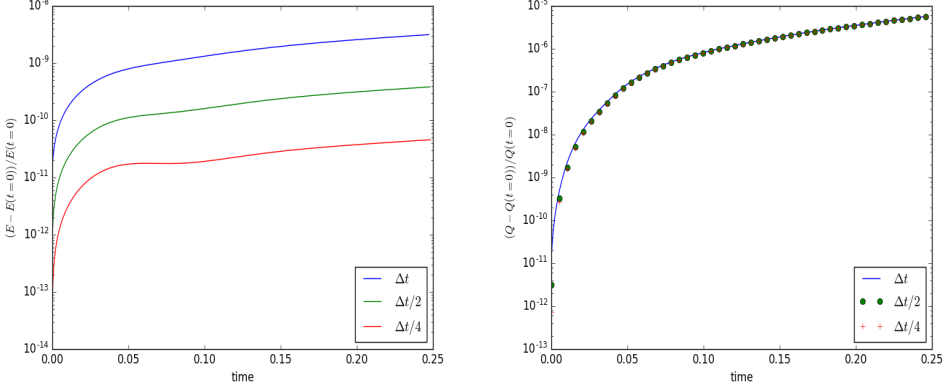


Fig. 6: Convergence of conservation errors for the energy, E (left) and potential enstrophy, Q (right) with time step Δt (inexact spatial integration).

tion becomes

$$\frac{d}{dt}(\beta_h^{(1)}, \beta_h^{(1)})_{\Omega_a} \tilde{u}_h^{(1)} = -(\beta_h^{(1)}, q_h^{(0)} \wedge \star F_h^{(1)})_{\Omega_a} + E_{1,2}(\gamma_h^{(2)}, \gamma_h^{(2)})_{\Omega_a} (\tilde{K}_h^{(2)} + g\tilde{h}_h^{(2)} + g\tilde{b}_h^{(2)}). \quad (67)$$

and the energy is correspondingly defined as $E = (h_h^{(2)}, K_h^{(2)} + 0.5gh_h^{(2)} + gb_h^{(2)})_{\Omega_a}$. The initial conditions are given as

$$h = H + 0.1 \tanh\left(\frac{1-y^2}{2}\right) \quad \vec{u} = \left(-\frac{\partial h}{\partial y}, 0\right) \quad (68)$$

and the orography as

$$b = \begin{cases} 0.0125(\cos(4\pi x/L) + 1)(\cos(4\pi y/L) + 1) & \text{if } |x| \leq L/4, |y| \leq L/4 \\ 0 & \text{otherwise} \end{cases} \quad (69)$$

with $-L/2 \leq x, y < L/2$, $L = 10$ and $f = g = H = 1.0$. In order to stabilize the potential enstrophy cascade, the anticipated potential vorticity $\hat{q}_h^{(0)}$ is removed from the rotational term in the momentum equation as given in (41). The test is run on 24×24 3rd order elements.

Figs. (7) and (8) show the evolution of the depth, vorticity and kinetic energy with time. While fast gravity waves radiate out from the topography as the solution adjusts, the vorticity field evolves on a slow time scale. The outline of the discontinuous 2-form elements of the orography field is visible in the 2-form depth field. Fig. (8) also shows the growth in vorticity ω , energy E , and potential enstrophy Q with time for varying values of the anticipated potential vorticity time scale $\Delta\tau$. As can be seen, vorticity conservation is preserved to machine precision independent of $\Delta\tau$, and the rate of energy growth is also similar for both values of $\Delta\tau$. The rates of potential enstrophy growth differ however, with $\Delta\tau = 0.02$ resulting in the growth of potential enstrophy (following

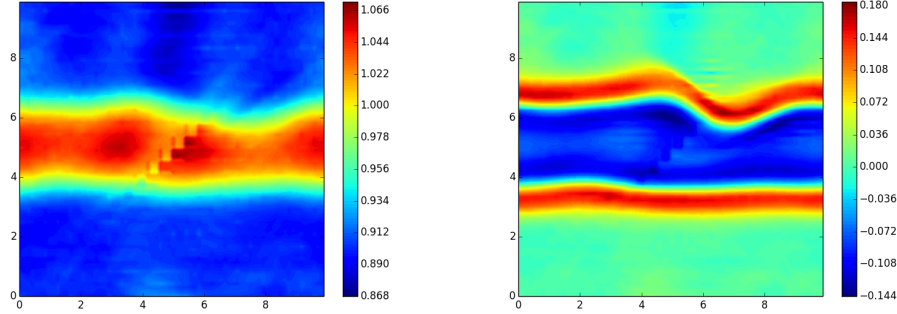


Fig. 7: Fluid depth h (left) and vorticity ω (right) fields for shear flow over orography at $t = 44$, $\Delta\tau = 0.02$.

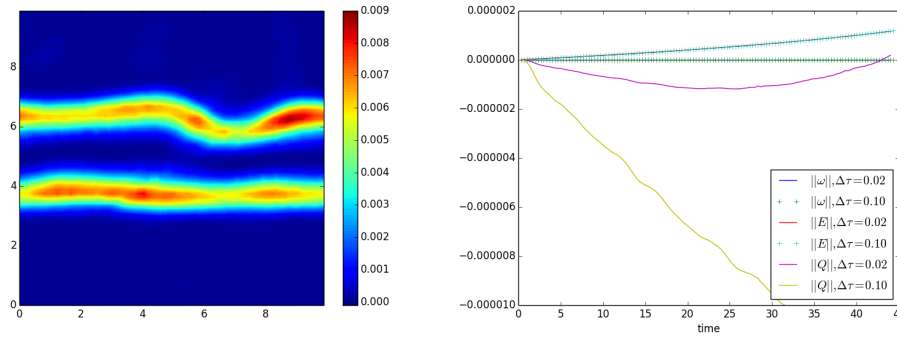


Fig. 8: Kinetic energy per unit volume K for shear flow over orography at $t = 44$, $\Delta\tau = 0.02$ (left), and growth of normalized vorticity ω , energy E and potential enstrophy Q with time for varying values of the anticipated potential vorticity coefficient $\Delta\tau$, where $\|A\| = (A(t) - A(t = 0))/A(t = 0)$.

an initial loss) while $\Delta\tau = 0.1$ results in the continued loss of Q . Note however that we cannot be certain that the potential enstrophy cascade is truly arrested for all time with the larger value of $\Delta\tau$. Any growth in potential enstrophy is perhaps a result of aliasing errors due to the inexact integration of the quadratic term $q_h^0 \wedge q_h^0$ in the potential enstrophy conservation equation.

5. Conclusion

In this paper we have built upon the work of previous authors in the development of compatible finite element methods for geophysical fluid dynamics [3, 4, 5] in order to present a shallow water solver which exactly conserves first order and second order moments using the mixed mimetic spectral element method [9, 10, 15]. The conservation of second order moments (energy and potential enstrophy) is subject to the truncation error in the time integration scheme, and the conservation of potential enstrophy also requires exact spatial integration, as shown by the conservation arguments and demonstrated for the test cases given above.

We note the performance constraints of the different diagnostic and prognostic equations as follows:

- Fluid depth, $h^{(2)}$: The continuity equation (37) is satisfied point wise in the strong form, and may be evaluated purely from the topology, with the divergence theorem satisfied exactly such that the change in fluid depth is simply the sum of the momentum on the adjacent 1-forms, multiplied by their orientation with respect to the given 2-form, and so is extremely fast to compute.
- Kinetic energy per unit volume, $K^{(2)}$: Since $K^{(2)}$ also exists on the discontinuous spaces of 2-forms, the weak form diagnostic equation (33) may be solved as a discontinuous Galerkin problem without the need for a global matrix solve.
- Potential vorticity, $q^{(0)}$: If we are prepared to sacrifice potential enstrophy conservation for an inexact quadrature rule, then the left hand side of (31) is diagonal due to the orthogonality of the 0-form basis functions $\alpha^{(0)}$. This again avoids the need for a global matrix solve
- Velocity, $u^{(1)}$ and momentum, $F^{(1)}$: Equations (37) and (32) require a global matrix solve, since their function space $\beta^{(1)}$ is continuous across element boundaries. The solution of these equations therefore represents the major computational bottleneck of the scheme.

While we have derived the potential vorticity from a diagnostic equation (31) in our current formulation, this could alternatively be derived from a prognostic equation (39). Doing so may have the added advantage of allowing for conservation of energy and potential enstrophy independent of time step via a time staggering of the variables, as has been previously shown for the Navier-Stokes equations [2].

6. Acknowledgements

David Lee would like to thank Drs. Chris Eldred and René Hiemstra for their helpful discussions and insights. This research was supported as part of the Launching an

Exascale ACME Prototype (LEAP) project, funded by the U.S. Department of Energy, Office of Science, Office of Biological and Environmental Research. Los Alamos Report LA-UR-17-24044

References

- [1] J. Thuburn, Some conservation issues for the dynamical cores of nwp and climate models, *J. Comp. Phys.* 227 (2008) 3715–3730.
- [2] A. Palha, M. Gerritsma, A mass, energy, enstrophy and vorticity conserving (MEEVC) mimetic spectral element discretization for the 2D incompressible Navier-Stokes equations, *J. Comp. Phys.* 328 (2017) 200–220.
- [3] C. Cotter, J. Shipton, Mixed finite elements for numerical weather prediction, *J. Comp. Phys.* 231 (2012) 7076–7091.
- [4] A. McRae, C. Cotter, Energy- and enstrophy-conserving schemes for the shallow-water equations, based on mimetic finite elements, *Q. J. R. Meteorol. Soc.* 140 (2014) 2223–2234.
- [5] A. Natale, J. Shipton, C. Cotter, Compatible finite element spaces for geophysical fluid dynamics, *Dynamics and Statistics of the Climate System* 1 (2016) 1–31.
- [6] A. Arakawa, V. Lamb, A potential enstrophy and energy conserving scheme for the shallow water equations, *Mon. Wea. Rev.* 109 (1981) 18–36.
- [7] C. Cotter, J. Thuburn, A finite element exterior calculus framework for the rotating shallow-water equations, *J. Comp. Phys.* 257 (2014) 1506–1526.
- [8] M. Taylor, A. Fournier, A compatible and conservative spectral element method on unstructured grids, *J. Comp. Phys.* 229 (2010) 5879–5895.
- [9] M. Gerritsma, Edge functions for spectral element methods, spectral and high order methods for partial differential equations, Springer (2011) 199–208.
- [10] J. Kreeft, M. Gerritsma, Mixed mimetic spectral element method for stokes flow: A pointwise divergence-free solution, *J. Comp. Phys.* 240 (2013) 284–309.
- [11] G. Vallis, *Atmospheric and Oceanic Fluid Dynamics: Fundamentals and Large-Scale Circulation*, Cambridge University Press, Cambridge, 2006.
- [12] J. Thuburn, T. Ringler, W. Skamarock, J. Klemp, Numerical representation of geostrophic modes on arbitrarily structured C-grids, *J. Comp. Phys.* 228 (2009) 8321–8335.
- [13] J. Thuburn, Numerical wave propagation on the hexagonal C-grid, *J. Comp. Phys.* 227 (2008) 5836–5858.
- [14] M. G. J. Kreeft, A. Palha, Mimetic framework on curvilinear quadrilaterals of arbitrary order, Cornell University Library.
- [15] R. Hiemstra, D. Toshniwal, R. Huijsmans, M. Gerritsma, High order geometric methods with exact conservation properties, *J. Comp. Phys.* 257 (2014) 1444–1471.
- [16] P. Bochev, M. Gerritsma, A spectral mimetic least-squares method, *Comput. Math. Appl.* 68 (2014) 1480–1502.
- [17] P. Bochev, J. Hyman, Principles of mimetic discretizations of differential operators, *MA Vol. Math. Appl.* 142 (2006) 89–119.
- [18] J. Thuburn, C. Cotter, A primal-dual mimetic finite element scheme for the rotating shallow water equations on polygonal spherical meshes, *J. Comp. Phys.* 290 (2015) 274–297.
- [19] R. Sadourny, C. Basdevant, Parameterization of subgrid scale barotropic and baroclinic eddies in quasi-geostrophic models: Anticipated potential vorticity method, *J. Atmos. Sci.* 42 (1985) 1353–1363.